atoms

MDPI

Article

Single and Double Electron Capture by 1–16 keV Sn^{4+} Ions Colliding on H_2

Emiel de Wit [1,2,†], Lennart Tinge [1,2,†], Klaas Bijlsma [1,2] and Ronnie Hoekstra [1,2,*]

[1] Zernike Institute for Advanced Materials, University of Groningen, Nijenborgh 3, 9747 AG Groningen, The Netherlands; emiel.de.wit@rug.nl (E.d.W.); l.tinge@rug.nl (L.T.); k.i.j.bijlsma@rug.nl (K.B.)
[2] Advanced Research Center for Nanolithography (ARCNL), Science Park 106, 1098 XG Amsterdam, The Netherlands
[†] These authors contributed equally to this work.

Abstract: Single and double electron capture cross-sections for collisions of $^{118}Sn^{4+}$ with molecular hydrogen have been measured in an energy range of 1 keV to 16 keV using a crossed-beam setup. The cross-sections are determined from measurements of charge-state-resolved ion currents obtained through a retarding field analyser. Remarkably, the single electron capture cross-sections for Sn^{4+} are more than a factor 3 smaller than the previously determined single electron capture cross-sections for Sn^{3+}–H_2 collisions and the double electron capture cross-sections are only about 20% smaller than the single electron capture cross-sections. These results are understood on the basis of potential energy curve crossings. The first active curve crossings for the Sn^{4+}–H_2 system happen at a relatively small internuclear distance of about 5.5 a.u., which should be compared to 8 a.u. for Sn^{3+} ions. Multi-channel Landau–Zener calculations have been performed for single electron capture and confirm these low cross-sections. The curve crossing for double electron capture by Sn^{4+} lies very close to the one for single electron capture, which may explain the single and double electron capture cross-sections being of similar magnitude.

Keywords: ion–molecule collisions; electron capture; Sn; molecular hydrogen

Academic Editor: Chihiro Suzuki

Received: 20 December 2024
Revised: 14 January 2025
Accepted: 21 January 2025
Published: 24 January 2025

Citation: de Wit, E.; Tinge, L.; Bijlsma, K.; Hoekstra, R. Single and Double Electron Capture by 1–16 keV Sn^{4+} Ions Colliding on H_2. *Atoms* **2025**, *13*, 12. https://doi.org/10.3390/atoms13020012

1. Introduction

Ever since the advent of sources for multiply charged ions in the 1980s, electron capture processes in collisions between low energy, multicharged ions and neutral targets have been studied, continuously advancing our understanding of induced electron dynamics. The ionic species used were mainly low-Z elements because of their relevance to astrophysics and fusion research and for being tractable to calculations with limited basis sets [1,2]. Currently, there is a shift in focus towards collisions with heavier, partially stripped elements which require more complicated and extensive calculations to include many-body effects. A medium-Z species of which the ions have recently attracted a lot of attention is Sn, because the 13.5 nm extreme ultraviolet (EUV) light driving modern nanolithography machines is generated by Sn ions in a laser-produced plasma (LPP) [3–5]. Such droplet LPP plasmas expand and emit Sn ions with energies up in to the keV energy range [6–8]. To protect the plasma-facing components, the LPP is embedded in an H_2 buffer gas which reduces the kinetic energy of the Sn ions [9–11]. Energy loss is known to depend on the charge state of the Sn ions [12]. However, cross-sectional data on electron capture is so far restricted to some data on Sn^{3+} and Sn^{2+} ions colliding on H_2 [13,14].

We have measured absolute cross-sections for single electron capture (SEC) and bound double electron capture (BDC) from H_2 by $Sn^{4+}([Kr]4d^{10}\ ^1S)$, i.e.,

$$Sn^{4+}(^1S) + H_2 \rightarrow Sn^{3+}(nl\ ^2L) + H_2{}^+, \quad (1)$$

and

$$Sn^{4+}(^1S) + H_2 \rightarrow Sn^{2+}(nln'l'\ ^1L) + 2H^+, \quad (2)$$

respectively. A contribution of autoionizing double capture (ADC), i.e.,

$$Sn^{4+}(^1S) + H_2 \rightarrow Sn^{3+}(nl\ ^2L) + 2H^+ + e^-, \quad (3)$$

is expected to be minute as this requires highly endothermic capture into doubly excited levels of Sn^{2+} and is therefore not considered. The energies of the Sn^{4+} ion beams used cover the range of 1 to 16 keV, partly overlapping with typical energies of Sn^{q+} ions escaping from a Sn-based laser-produced plasma, e.g., [6,15,16]. The energy range includes the regime in which the Franck–Condon approximation, commonly used in charge transfer models, breaks down [14], which makes for challenging calculations.

2. Experimental Methods

The cross-sections presented in this work are extracted from the measurement of the charge state distribution resulting from a monoenergetic Sn^{4+} ion beam traversing a beam of H_2 in a crossed-beam-type setup (CHEOPS, charge exchange observed by particle spectroscopy). The CHEOPS rig is a permanent fixture of the Zernike low-energy ion beam facility (ZERNIKELEIF) at the University of Groningen. The ion beams available at the facility are extracted from an electron cyclotron resonance ion source (ECRIS). Inside the source, a crucible filled with solid Sn is heated to evaporate Sn atoms into the central source plasma of He.

The ECRIS is floated at a high voltage of a maximum of 25 kV, so the extracted ions can be accelerated to a maximum kinetic energy of $25q$ keV, where q is the charge state of the ion. The ions are guided into a 110° analysing magnet, which selects ions of a certain mass-over-charge ratio m/q. For this work, the analysing magnet is set to select $^{118}Sn^{4+}$ rather than the more abundant isotope $^{120}Sn^{4+}$ due to the presence of NO^+ ions at an m/q of 30. After the analyzing magnet, the ion beam is injected into the central beam line, from which, by means of a 45° dipole magnet, the ions are bent into the direction of the crossed-beam setup.

2.1. The Crossed-Beam Setup

The crossed-beam setup (see Figure 1) used for this work was previously used for measurements of $Sn^{3+} + H_2$ collisions and is described in detail in references [13,17]. To allow measurements to be performed at low kinetic energies, the setup is placed on a high voltage (HV) platform. The energy of the ions inside the collision chamber is thus determined by the potential difference between the ion source and the HV platform. In order to prevent the divergence of the ion beam due to a sudden jump in potential as it enters the collision chamber, a six-element electrostatic deceleration lens is used to contain the ion beam during deceleration. Inside the collision chamber, the Sn^{4+} ions collide with an effusive H_2 gas beam, which is injected through a 100 mm long capillary with an inner diameter of 1 mm, located 1 mm above the center of the ion beam. After collision, the ion beam is collected and analyzed by a Retarding Field Analyzer (RFA). This RFA consists of a Faraday Cup (FC) placed behind a number of electrodes, which, through an applied retarding voltage, produce an electrostatic barrier qU_{ret} to the $q+$ ions; only ions with an energy $E > qU_{ret}$ are able to surpass the barrier and be collected by the

FC. Charge-state-resolved ion currents are obtained by varying the retarding potential of the RFA.

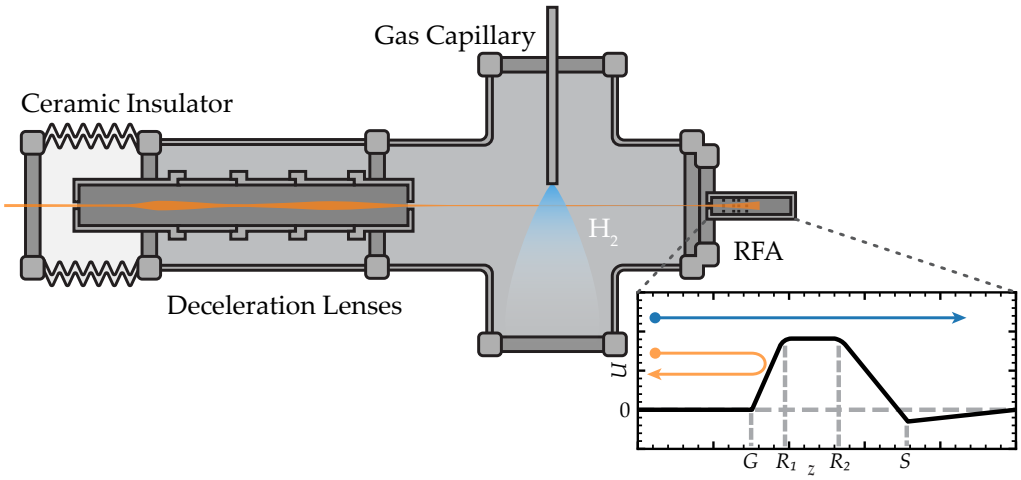

Figure 1. Schematic overview of the relevant parts of CHEOPS. The crossed-beam setup floats at a high voltage and is insulated from the grounded beamline by a ceramic vacuum break. After deceleration and focusing by the deceleration lenses, the ions (indicated in orange) cross with a H_2 target beam after which the beam is collected and its charge state analyzed by a Retarding Field Analyzer (RFA). The inset (bottom right) sketches the potential experienced by ions entering the RFA. Between R_1 and R_2, a retarding potential U_{ret} is applied which imposes an energy barrier on qU_{ret} ions. Only ions (blue arrow) with energies $> qU_{ret}$ can overcome the barrier and be collected in the Faraday cup; ions with a lower energy (orange arrow) will be repelled by the barrier.

2.2. Measurement Procedure

The determination of the SEC and BDC cross-sections, σ_{43} and σ_{42}, respectively, requires accurate measurements of the Sn^{4+}, Sn^{3+} and Sn^{2+} ion currents after an initially pure Sn^{4+} beam has passed through the gas target at multiple densities. The Sn^{4+}, Sn^{3+} and Sn^{2+} charge state distribution can be described by the following system of differential equations:

$$\begin{pmatrix} \frac{dN^{4+}}{dz} \\ \frac{dN^{3+}}{dz} \\ \frac{dN^{2+}}{dz} \end{pmatrix} = n(z) \begin{pmatrix} -(\sigma_{43}+\sigma_{42}) & 0 & 0 \\ \sigma_{43} & -(\sigma_{32}+\sigma_{31}) & 0 \\ \sigma_{42} & \sigma_{32} & -(\sigma_{21}+\sigma_{20}) \end{pmatrix} \begin{pmatrix} N^{4+}(z) \\ N^{3+}(z) \\ N^{2+}(z) \end{pmatrix}, \quad (4)$$

with N^{q+} being the number of ions of charge state q, $\sigma_{q,q-1}, \sigma_{q,q-2}$ being the single and double electron capture cross-sections, respectively, n is the target density and z is the position along the ion beam trajectory. The total trajectory length through the target gas is L. In the single-collision regime, only the left column of the matrix in Equation (4) needs to be considered. The electron capture cross-sections for Sn^{3+} and Sn^{2+} ions in columns 2 and 3 contain the effect of double collisions on the charge state distribution. Based on the work by Bijlsma et al. [14], we assume σ_{21} and σ_{20} to be negligibly small compared to the Sn^{4+} and Sn^{3+} cross-sections. The σ_{21} cross-section is significant only if the Sn^{2+} is produced in its metastable $Sn^{2+}(4d^{10}5s5p\ ^3P)$ term. This is unlikely in BDC by Sn^{4+} because it would violate the conservation of spin, as will be discussed in the next section. For practical reasons, the total electron capture cross-sections $\sigma_q = \sigma_{q,q-1} + \sigma_{q,q-2}$ for Sn^{q+} ions are introduced and the integral target density is taken to be proportional to the pressure (P), i.e., $\int_0^L n(z)dz = \beta P$. The value of the proportionality constant β is obtained from calibration to a collision system with well-established single and double electron capture cross-sections; here, we use the $O^{6+} + H_2$ system [18]. With these ingredients, the solutions to the set of differential equations are given by the following:

$$N^{4+}(L) = N_0\, e^{-\sigma_4 \beta P}, \tag{5a}$$

$$N^{3+}(L) = N_0 \frac{\sigma_{43}}{\sigma_4 - \sigma_3}\left(e^{-\sigma_3 \beta P} - e^{-\sigma_4 \beta P}\right), \tag{5b}$$

$$N^{2+}(L) = N_0 \frac{\sigma_{32}\sigma_{43}}{\sigma_3(\sigma_4 - \sigma_3)}\left(1 - e^{-\sigma_3 \beta P}\right) - N_0 \frac{\sigma_4(\sigma_{32} - \sigma_{42}) + \sigma_{31}\sigma_{42}}{\sigma_4(\sigma_4 - \sigma_3)}\left(1 - e^{-\sigma_4 \beta P}\right). \tag{5c}$$

Equation (5a) allows for the determination of the total electron capture cross-section σ_4. To account for the effects of double collisions, we define a ratio f of 2+ over 3+ ions as given by Equations (5c) and (5b). As the pressures we measure at are reasonably low, this ratio is well described by a Taylor series around $P = 0$:

$$f(P) = \frac{N^{2+}}{N^{3+}} = \frac{\sigma_{42}}{\sigma_{43}} + \frac{\sigma_{32}\sigma_4}{2\sigma_{43}}\left(1 + \frac{\sigma_{31}\sigma_{42}}{\sigma_{32}\sigma_4}\right)\beta P + \mathcal{O}(P^2). \tag{6}$$

In the limit of zero density (single collision regime), f is equal to the ratio f_0 of the cross-sections for double- and single-electron capture by Sn^{4+}.

In summary,

$$\sigma_4 = \frac{-\ln\left(\frac{N^{4+}}{N_0}\right)}{\beta P}, \qquad \sigma_{43} = \frac{\sigma_4}{1 + f_0}, \qquad \sigma_{42} = f_0 \sigma_{43}, \tag{7}$$

with f_0 the value of the ratio f at zero pressure (density). We obtain f_0 and $\frac{df}{dP}$ from an extrapolated least-squares fit to our measured ratios N^{2+}/N^{3+}. An example of this extrapolation, together with all resulting ratios f_0 determined over the full range of investigated kinetic energies, are shown in Figure 2.

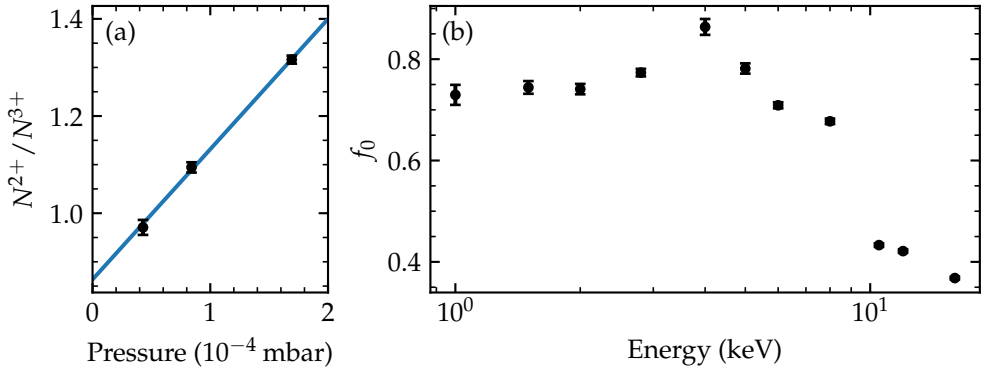

Figure 2. (**a**) The ratio f of measured Sn^{2+} ions to Sn^{3+} ions generated from a 4 keV Sn^{4+} ion beam measured at three H_2 pressures. The blue line is a least-squares fit to the data. The y-intercept, f_0, is used in Equation (7). (**b**) The ratio f_0 between SEC and BDC cross-sections as a function of energy of the incoming Sn^{4+} ions. The error bars shown indicate the statistical errors of the measurements.

3. Results and Discussion

The measured cross-sections for Sn^{4+} colliding with H_2 are collected in Figure 3. In the energy range of 1 keV to 8 keV, the SEC and BDC cross-sections are of similar magnitude. Above 8 keV, the cross-sections for SEC and BDC diverge as the SEC cross-sections increase with energy while the BDC cross-sections decrease. The total electron capture cross-section (σ_4) is basically constant as shown by the dotted grey line. The value of 20×10^{-16} cm^2 for the total electron capture cross-section is remarkably low. It is only half of the SEC cross-section for Sn^{3+} collisions on H_2; see Figure 3.

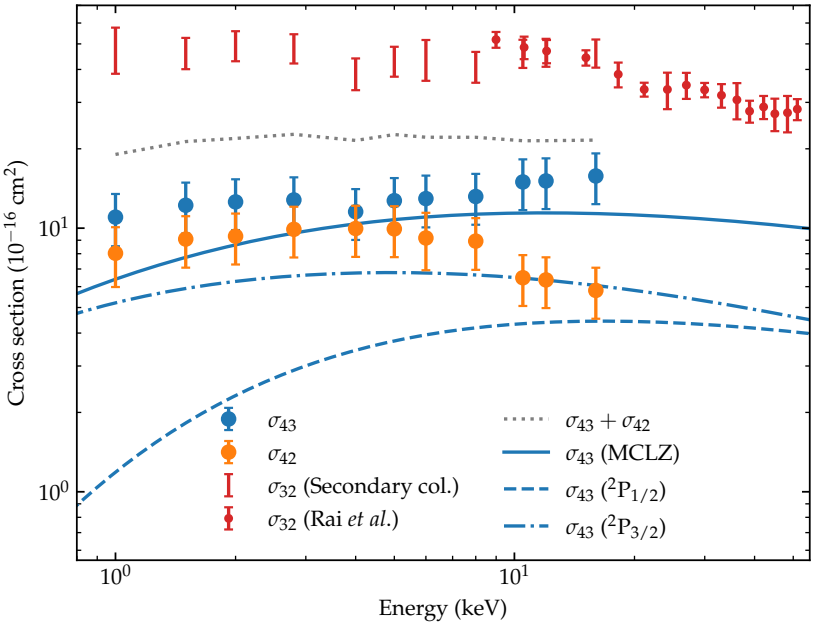

Figure 3. Experimentally obtained cross-sections for SEC by $Sn^{4+} + H_2$ (blue symbols) and BDC by $Sn^{4+} + H_2$ (orange symbols). The error bars in our σ_{43} and σ_{42} values represent the statistical uncertainty. The 7% systematic uncertainty in our calibration of the proportionality constant β is not included. The sum of σ_{43} and σ_{42} is shown by the dashed grey line. The results of multi-channel Landau–Zener calculations of single electron capture (σ_{43}) are shown by the solid blue line. The dashed blue lines indicate the individual contributions by the $4d^{10}5p\ ^2P_{1/2,\,3/2}$ levels to σ_{43}. For a consistency check of our data, indirect σ_{32} cross-sections (red bars), extracted from the double collision contributions to our pressure dependent measurements, (see Figure 2), are compared to the σ_{32} cross-sections measured by Rai et al. [13], which are given by the red dots.

To check the consistency between our present findings for Sn^{4+} and previous results for Sn^{3+}, we extracted σ_{32} cross-sections from the double collision contribution to our measurements of the ratio f of 2+ and 3+ ions produced, cf. Equation (6). From that equation, one sees that σ_{32} can be extracted from the slope of f as a function of gas pressure ($\frac{df}{dP}$). The values of ($\frac{df}{dP}$) are directly available from the least-squares fits used to extrapolate f to zero pressure; see Figure 2a. From Equation (6), it is derived that

$$\sigma_{32} = \frac{2\sigma_{43}}{\sigma_4}\left(1 + \frac{\sigma_{31}\sigma_{42}}{\sigma_{32}\sigma_4}\right)^{-1}\frac{1}{\beta}\frac{df}{dP}. \tag{8}$$

The second correction term between brackets which includes σ_{32} is negligibly small. From Figure 3, one can extract that the ratio $\frac{\sigma_{42}}{\sigma_4}$ is at maximum ~0.4. The ratio $\frac{\sigma_{31}}{\sigma_{32}}$ was determined by Rai et al. [13] to be constant over the energy range of 9 keV to 51 keV and to be small, i.e., ~0.1. At low energies, $\frac{\sigma_{31}}{\sigma_{32}}$ might change, but even if it would increase threefold when going down to 1 keV, the effect on the σ_{32} cross-sections would be in the order of ~10%. The resultant estimates of the σ_{32} cross-sections are shown in Figure 3 as red uncertainty bars. In the region of overlapping collision energies, we find good agreement between our measurements and those performed by Rai et al. [13], thereby proving the consistency between our present data for Sn^{4+} and the earlier data set on Sn^{3+}.

Before continuing the discussion of our data, we would like to point out that the consistency with the earlier σ_{32} results indicates that metastables do not affect our data appreciably. The Sn^{4+} ion beam may contain a fraction of metastables, having a $[Kr]4d^9 5s$ configuration. The lifetimes of the $^1D_2$, $^3D_1$, and $^3D_2$ 40 µs, 1430 s and 171 µs, respectively [19,20]. For $^3D_3$, no lifetime information is available. The flight time from the source to collision chamber is ~43 µs, meaning that only the $^1D_2$ and $^3D_2$ ions experience signifi-

cant decay (∼67% and ∼23%). Therefore, although we have a long flight time, it does not exclude the presence of metastables. To assess a presence of metastables, the ECR source has been operated at widely different settings which did not lead to significant changes in the data. This indicates to us that the fraction of metastables is small or has similar cross-sections as the ground state Sn^{4+}. This conclusion is supported by our determination of the σ_{32} cross-sections, which depend on the ratio of single and double electron capture (σ_{42}/σ_{43}). The one electron capture signal is used to put σ_{43} on an absolute scale. All other cross-sections are linked to this calibration. A change in σ_{43} without a change in σ_{42}/σ_{43} as a result of a metastable fraction in the beam would result in an overall shift in all cross-sections, reducing the consistency between our σ_{32} and earlier measurements. Therefore, we are convinced that metastables do not affect the presented cross-sections appreciably. However, we cannot exclude the presence of metastables, because their cross-sections might be of similar magnitude to the ones of ground state Sn^{4+} ions.

The SEC cross-sections of Sn^{4+}, being about a factor of three smaller than the ones of Sn^{3+}, can be explained by considering the potential energy diagram of $Sn^{4+} + H_2$ collisions, which is shown in Figure 4. From the figure it is seen that the curve crossings with the $Sn^{3+}(4d^{10}5p\,^2P_{1/2,\,3/2})$ channels will be the most active ones. The crossing of the entrance channel with the $Sn^{3+}(4d^{10}5d\,^2D)$ channel lies very far out and therefore is crossed adiabatically. The crossings with the $Sn^{3+}(4d^{10}5p\,^2P_{1/2,\,3/2})$ levels are located at an internuclear distance of approximately 5.5 a.u. This distance of 5.5 a.u. should be compared to 8.5 a.u. for the effective channel crossing in collisions of Sn^{3+} ions on H_2 [13]. The ratio of the internuclear distances of the crossing points for Sn^{3+} and Sn^{4+} squared is ∼2.5 in favor of Sn^{3+}, which is a fair agreement with the measured factor of ∼3.

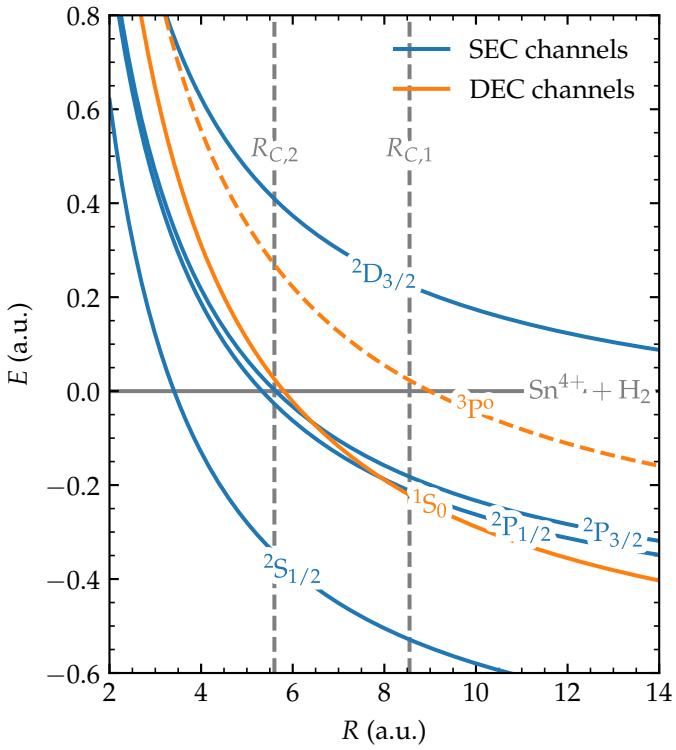

Figure 4. Potential (Coulomb) energy curves of the relevant $Sn^{4+} + H_2$ (gray), $Sn^{3+} + H_2{}^+$ (blue) and $Sn^{2+} + 2\,H^+$ (orange) electronic states as functions of the internuclear distance between the Sn ion and the H_2 target (dashed line indicates a spin-forbidden final state). The vertical dashed line indicates the over-barrier crossings $R_{C,1}, R_{C,2}$ for single and double electron capture, respectively, used to indicate approximately where resonant capture can start to take place [21]. The term symbols for the Sn ions after separation are indicated in the figure.

To obtain further insight in SEC from H_2 by Sn^{4+}, we have performed multi-channel Landau–Zener (MCLZ) calculations following [22,23]. In the model, the $Sn^{4+}(^1S_0) + H_2$ entrance channel and the four $Sn^{3+} + {H_2}^+$ single electron capture channels that are shown in Figure 4 have been included. In order to account for the molecular nature of the target, we included the Franck–Condon factor corresponding to a transition to the most likely $v' = 2$ vibrational state of ${H_2}^+$ [24] into the coupling matrix elements H_{12}, as proposed by Olson and Salop [23]. Instead of the initial prefactor to coupling elements, primarily based on one-electron systems, the empirical prefactor determined by Kimura et al. [22] for collisions on He targets was used. Additionally, the coupling matrix elements are corrected by multiplication with a factor f_{nl}, introduced by Taulbjerg [25] for partially stripped ions to account for the non-degenerate nature of the l states within a specific n shell.

Notwithstanding the approximations inherent to the one-dimensional Landau–Zener model, the calculations agree with the magnitude of the measured single-electron capture cross-sections and indicate that it is indeed the $^2P_{1/2}$ and $^2P_{3/2}$ levels that in between them carry the total SEC cross-section. The corresponding channel-selective and total cross-sections are shown in Figure 3. For energies above approximately 2 keV, the model results are in good agreement with the energy dependence observed in the measurements. Concerning the absolute values, the model falls short by about 30%. Below 2 keV, the difference slowly increases to almost 50% at 1 keV. The same trend, although stronger, has been observed for $Sn^{2+} + H_2$ [14] and was ascribed to the breakdown of the Franck–Condon approximation.

At almost the same internuclear distance as the $Sn^{3+}(^2P)$ crossings, a crossing occurs between the entrance channel and the $Sn^{2+}(4d^{10}5s^{2}\,{}^1S_0) + 2\,H^+$ BDC channel. This level is expected to be the main if not sole contributor to BDC by Sn^{4+}, as spin conservation (singlet entrance channel) inhibits the population of the next BDC channel which is a triplet ($Sn^{2+}(4d^{10}5s5p\,{}^3P)$). The potential energy diagram in Figure 4 shows that the $5s^2\,{}^1S$ BDC channel also crosses the ^2P_J levels, which opens the option for electron transfer between SEC and BDC channels on the way-out of the collision. These close crossings raise the question whether double electron capture in this system is facilitated primarily by simultaneous (one-step) or successive (two-step) electron-capture processes [26] and might help to explain the ratio between SEC and BDC by Sn^{4+}; see Figure 2b, which maximizes at energies near 4 keV at a value slightly above 0.8.

4. Conclusions

We have measured cross-sections of single and double electron capture by Sn^{4+} ions from molecular hydrogen in an energy range relevant to the plasma expansion processes in the EUV sources of modern photolithography machines. The cross-sections are extracted from charge-separated ion currents in a crossed-beam experiment of Sn^{4+} with H_2. Remarkably, the SEC and DEC cross-sections are of similar magnitude and much lower than previously measured cross-sections of SEC by Sn^{3+}. Our measurements are consistent with earlier work, as is demonstrated by comparing the known σ_{32} cross-sections with those extracted from double collisions in our experiment. The low SEC cross-sections are explained by the absence of potential curve crossings at larger internuclear distances: the first suitable crossings are when the $Sn^{3+}(4d^{10}5p\,{}^2P_{1/2,\,3/2}) + {H_2}^+$ channels cross with the entrance channel at about 5.5 a.u. Multi-channel Landau–Zener calculations of σ_{43} are found to be in fair agreement with the measured SEC cross-sections. The BDC capture channel crosses both the entrance channel and SEC channels in the direct vicinity of the crossing of the SEC and entrance channel; this may imply a strong intermixing between SEC and BDC and could therefore require more advanced calculations.

Author Contributions: Conceptualization, R.H.; methodology, E.d.W., L.T. and K.B.; software, E.d.W., L.T. and K.B.; investigation, E.d.W. and L.T.; resources, R.H.; data curation, E.d.W. and L.T.; writing—original draft preparation, E.d.W.; writing—review and editing, E.d.W., L.T., K.B. and R.H.; visualization, E.d.W. and L.T.; supervision, R.H.; project administration, R.H. All authors have read and agreed to the published version of the manuscript.

Funding: This research received no external funding.

Data Availability Statement: The raw data supporting the conclusions of this article will be made available by the authors on request.

Acknowledgments: The experimental work was carried out at the ZERNIKELEIF facility in the Zernike Institute for Advanced Materials of the University of Groningen as part of the research portfolio of the Advanced Research Center for Nanotlithography (ARCNL), a public-private partnership between the University of Amsterdam (UvA), the Vrije Universiteit Amsterdam (VU), the University of Groningen (RuG), the Netherlands organization for Scientific Research (NWO) and the semiconductor equipment manufacturer ASML.

Conflicts of Interest: The authors declare no conflicts of interest.

References

1. Janev, R.K.; Winter, H. State-selective electron capture in atom-highly charged ion collisions. *Phys. Rep.* **1985**, *117*, 265–387. [CrossRef]
2. Fritsch, W.; Lin, C.D. The semiclassical close-coupling description of atomic collisions: Recent developments and results. *Phys. Rep.* **1991**, *202*, 1–97. [CrossRef]
3. O'Sullivan, G.; Li, B.; D'Arcy, R.; Dunne, P.; Hayden, P.; Kilbane, D.; McCormack, T.; Ohashi, H.; O'Reilly, F.; Sheridan, P.; et al. Spectroscopy of highly charged ions and its relevance to EUV and soft x-ray source development. *J. Phys. B At. Mol. Opt. Phys.* **2015**, *48*, 144025. [CrossRef]
4. Banine, V.Y.; Koshelev, K.N.; Swinkels, G.H.P.M. Physical processes in EUV sources for microlithography. *J. Phys. D Appl. Phys.* **2011**, *44*, 253001. [CrossRef]
5. Torretti, F.; Sheil, J.; Schupp, R.; Basko, M.M.; Bayraktar, M.; Meijer, R.A.; Witte, S.; Ubachs, W.; Hoekstra, R.; Versolato, O.O.; et al. Prominent radiative contributions from multiply-excited states in laser-produced tin plasma for nanolithography. *Nat. Commun.* **2020**, *11*, 2334. [CrossRef]
6. Fujioka, S.; Nishimura, H.; Nishihara, K.; Murakami, M.; Kang, Y.G.; Gu, Q.; Nagai, K.; Norimatsu, T.; Miyanaga, N.; Izawa, Y.; et al. Properties of ion debris emitted from laser-produced mass-limited tin plasmas for extreme ultraviolet light source applications. *Appl. Phys. Lett.* **2005**, *87*, 241503. [CrossRef]
7. Murakami, M.; Kang, Y.G.; Nishihara, K.; Fujioka, S.; Nishimura, H. Ion energy spectrum of expanding laser-plasma with limited mass. *Phys. Plasmas* **2005**, *12*, 062706. [CrossRef]
8. Doggett, B.; Lunney, J.G. Expansion dynamics of laser produced plasma. *J. Appl. Phys.* **2011**, *109*, 093304. [CrossRef]
9. Nakamura, D.; Tamaru, K.; Hashimoto, Y.; Okada, T.; Tanaka, H.; Takahashi, A. Mitigation of fast ions generated from laser-produced Sn plasma for extreme ultraviolet light source by H_2 gas. *J. Appl. Phys.* **2007**, *102*, 123310. [CrossRef]
10. Rai, S.; Bijlsma, K.I.; Poirier, L.; Wit, E.d.; Assink, L.; Lassise, A.; Rabadán, I.; Méndez, L.; Sheil, J.; Versolato, O.O.; et al. Evidence of production of keV Sn+ ions in the H2 buffer gas surrounding an Sn-plasma EUV source. *Plasma Sources Sci. Technol.* **2023**, *32*, 035006. [CrossRef]
11. Bartlett, N.; Herschberg, A.; Crouse, J.; Dallal, T.; Nuttal, J.; Stahl, J.; Braaksma, N.; Ruzic, D. Elastic scattering cross sections and transport of tin ions in extreme ultraviolet lithography sources. *Phys. Scr.* **2024**, *99*, 065411. [CrossRef]
12. Abramenko, D.B.; Spiridonov, M.V.; Krainov, P.V.; Krivtsun, V.M.; Astakhov, D.I.; Medvedev, V.V.; van Kampen, M.; Smeets, D.; Koshelev, K.N. Measurements of hydrogen gas stopping efficiency for tin ions from laser-produced plasma. *Appl. Phys. Lett.* **2018**, *112*, 164102. [CrossRef]
13. Rai, S.; Bijlsma, K.I.; Rabadán, I.; Méndez, L.; Wolff, P.A.J.; Salverda, M.; Versolato, O.O.; Hoekstra, R. Charge exchange in collisions of 1–100-keV Sn^{3+} ions with H_2 and D_2. *Phys. Rev. A* **2022**, *106*, 012804. [CrossRef]
14. Bijlsma, K.; Oltra, L.; de Wit, E.; Assink, L.; Rabadán, I.; Méndez, L.; Hoekstra, R. Electron Capture from Molecular Hydrogen by Metastable Sn^{2+*} Ions. *Atoms* **2024**, *12*, 9. [CrossRef]
15. Chen, Z.; Wang, X.; Zuo, D.; Wang, J. Investigation of ion characteristics in CO_2 laser irradiating preformed tin-droplet plasma. *Laser Part. Beams* **2016**, *34*, 552–561. [CrossRef]

16. Hemminga, D.J.; Poirier, L.; Basko, M.M.; Hoekstra, R.; Ubachs, W.; Versolato, O.O.; Sheil, J. High-energy ions from Nd:YAG laser ablation of tin microdroplets: Comparison between experiment and a single-fluid hydrodynamic model. *Plasma Sources Sci. Technol.* **2021**, *30*, 105006. [CrossRef]
17. Bijlsma, K.; de Wit, E.; Kleinsmit, A.; Lalkens, E.; Assink, L.; Salverda, M.; Oltra, L.; Rabadán, I.; Méndez, L.; Versolato, O.O.; et al. Electron capture in low-energy collisions of Sn^{3+} ions with H_2 and D_2. 2024, *in preparation*.
18. Machacek, J.R.; Mahapatra, D.P.; Schultz, D.R.; Ralchenko, Y.; Chutjian, A.; Simcic, J.; Mawhorter, R.J. Measurement and calculation of absolute single- and double-charge-exchange cross sections for O^{6+} ions at 1.17 and 2.33 keV/u impacting He and H_2. *Phys. Rev. A* **2014**, *90*, 052708. [CrossRef]
19. Singh, N.; Goyal, A. Energy levels, transition data and collisional excitation cross-section of Sn^{3+} and Sn^{4+} ions. *J. Electron Spectrosc. Relat. Phenom.* **2020**, *244*, 146982. [CrossRef]
20. Kramida, A.; Ralchenko, Y. *NIST Atomic Spectra Database, NIST Standard Reference Database 78*; NIST: Washington, DC, USA, 1999. [CrossRef]
21. Niehaus, A. A classical model for multiple-electron capture in slow collisions of highly charged ions with atoms. *J. Phys. B At. Mol. Phys.* **1986**, *19*, 2925. [CrossRef]
22. Kimura, M.; Iwai, T.; Kaneko, Y.; Kobayashi, N.; Matsumoto, A.; Ohtani, S.; Okuno, K.; Takagi, S.; Tawara, H.; Tsurubuchi, S. Landau-Zener Model Calculations of One-Electron Capture from He Atoms by Highly Stripped Ions at Low Energies. *J. Phys. Soc. Jpn.* **1984**, *53*, 2224–2232. [CrossRef]
23. Olson, R.E.; Salop, A. Electron transfer between multicharged ions and neutral species. *Phys. Rev. A* **1976**, *14*, 579–585. [CrossRef]
24. Wacks, M.E. Franck-Condon factors for the ionization of H_2, HD, and D_2. *J. Res. Natl. Bur. Stand. Sect. A Phys. Chem.* **1964**, *68A*, 631. [CrossRef]
25. Taulbjerg, K. Reaction windows for electron capture by highly charged ions. *J. Phys. B At. Mol. Phys.* **1986**, *19*, L367. [CrossRef]
26. Barat, M.; Roncin, P. Multiple electron capture by highly charged ions at keV energies. *J. Phys. B At. Mol. Opt. Phys.* **1992**, *25*, 2205. [CrossRef]